Heliyon 8 (2022) e12633

Contents lists available at ScienceDirect

Heliyon

journal homepage: www.cell.com/heliyon

Research article

Fabrication of novel buckypaper metal oxide nano-catalysis glycerol carbonate/MWCNTs membrane for efficient removal of heavy metals

Seham S. Alterary [a,*], Ahmed A. Alshahrani [b], Shahad A. Alsahli [a]

[a] Department of Chemistry, College of Science, King Saud University, Riyadh, P.O. Box 11495, Saudi Arabia
[b] National Centre for Radiological Applications Technology, King Abdul Aziz City for Science and Technology, Riyadh, 11442, Saudi Arabia

ARTICLE INFO

Keywords:
Buckypaper membrane
Heavy metals
Water treatments
Metal oxides nanoparticles
Surfactants

ABSTRACT

This study describes the fabrication of novel buckypaper membranes through the dispersion of multi-walled carbon nanotubes (MWCNTs) in the presence of surfactants metal oxide nano-catalysis Zinc oxide and magnesium oxide (ZnO and MgO) glycerol carbonate separately. Following vacuum filtration of the scattered solutions, self-supporting membranes known as buckypapers (BPs) were produced. The suggested membranes were employed for the efficient removal of heavy metals. The obtained data indicated that the incorporation of both glycerol carbonates prepared by two different nano metal oxides enhanced the permeability of MWCNTs membranes rejection efficiency. The characterization of the synthesized metal oxide nanoparticles, as well as the physicochemical and morphological properties of the membranes, were investigated. The rejection capabilities of membranes for the heavy metal ions were examined. Moreover, the suggested MWCNTs/ZnO nano-catalyst glycerol carbonate BP membrane displayed high rejection efficiency for heavy metals (Cd^{2+}, Cu^{2+}, Co^{2+}, Ni^{2+}, and Pb^{2+}) than that prepared from the MgO nano-catalyst one.

1. Introduction

Expeditious industrial development along water sources has put additional strain on these sources and caused the water is becoming more polluted and the environmental health is deteriorating [1]. As the population of the planet grows, industrialization is rapidly taking place and becoming the primary cause of water contamination [2]. Heavy metal-contaminated wastewater poses a significant difficulty because it is poisonous and not biodegradable [3]. Heavy components were discovered by researchers in agricultural products in industrial areas. These products can be found on the dining table of the average consumer and pose major health hazards [4]. Moreover, various techniques are applied to remove heavy metals from wastewater, including direct regeneration of ion exchange resins [5], scaled-up microbial electrolysis cells [6], chemical oxidation [7], adsorption [8], and membrane filtration [9]. Because of its simplicity and low cost, the membrane filtering process is highly recommended. Impurities are removed from water via membrane filtration by exerting pressure across the membrane. Depending on the amount of pressure applied and the size of the undesirable component, membrane filtration techniques such as microfiltration (MF), reverse osmosis (RO), ultrafiltration (UF), and nanofiltration (NF) can be used [10]. NF stands out as a wonderful option to remove the tiniest impurities since it has a greater rejection rate and quicker water flux than the other procedures. It operates under lower pressure than RO, resulting in greater energy efficiency. It also removes materials with lower densities than UF and MF [11]. Additionally, polymer-based membranes are necessary for water purification in NF. Due to their high adsorption capacity, economic effectiveness, and ease of processing, polymeric membranes had garnered interest [12]. However, they have poor mechanical qualities that make it impossible to use them in portable water treatment systems or large-scale water treatment procedures. Due to the several desired qualities MWCNTs possess, such as their excellent mechanical properties, conductivity, large surface area, thermal and chemical stability, and ease of fabrication, MWCNTs have therefore been used to reinforce polymeric membranes as a solution to this problem [13]. MWCNTs are dissolved in the polymeric solution and vacuum filtered to create buckypapers, which are self-supporting carbon nanotubes (CNT)-based membranes (BP). Numerous researchers have looked into BPs' capacity to treat water; they

* Corresponding author.
E-mail address: salterary@ksu.edu.sa (S.S. Alterary).

https://doi.org/10.1016/j.heliyon.2022.e12633
Received 18 August 2022; Received in revised form 3 November 2022; Accepted 20 December 2022

have demonstrated excellent results in adsorbing unwanted substances from wastewater [14, 15, 16, 17]. As a result, they are an excellent alternative to conventional active carbon-based portable water treatment devices in homes and factories.

Nanoscale materials, particularly metal oxide nanoparticles, are a distinct class of materials with unique physicochemical properties that have a wide range of applications in science, including catalysis [18], renewable energy [19], and removal of environmental pollution [20], and photodegradation [21]. The astonishing physical and chemical properties of Zinc oxide nanoparticles (ZnONPs) and Magnesium oxide nanoparticles (MgONPs), encourage their prospective in various applications including, solar cells [22, 23], sustainable fuels [24, 25], sensors [26, 27], nanoelectronics devices [28, 29], environmental remediation [30, 31]. Furthermore, metal oxide-based catalysis is also an important key in the reaction processes in various chemical reactions such as alkylation, the transesterification in the chemical industry [32].

Glycerol carbonate (GC) is an essential raw ingredient in the chemical industry. This small molecule, with a molar weight of 118.09 g/mol, is one of the glycerol derivatives attracting increased scientific and industrial interest due to its good physical and chemical characteristics, as well as its broad reactivity. Long-term glycerol-urea interaction results in the formation of glycerol carbonate [33]. Glycerol carbonate synthesis provides an alternate method for revaluing waste glycerol produced in huge quantities during biodiesel manufacturing. The fatty acid methyl esters generated from the transesterification of vegetable oils with methanol are known as biodiesel. Biodiesel can be made from a variety of feedstocks, but it always produces glycerol as a by-product, which accounts for one-tenth of biodiesel production [34].

The reaction of glycerol with urea to produce glycerol carbonate (sometimes referred to as glycerin carbonate or 4-hydroxymethyl-2-oxo-1,3-dioxolane) is a fascinating technique that takes advantage of two inexpensive and easily available raw ingredients. The most important process involving the chemical use of carbon dioxide (CO_2) is the reaction between CO_2 and ammonia (NH_3), which produces urea [35]. The use of CO_2 as a platform chemical is a simple and long-term solution to the problem of decreasing CO_2 emissions impact. Glycerol carbonate and NH_3 are produced during the glycerolysis of urea. By reacting with carbon dioxide, this ammonia can be easily transformed back to urea. As a result, this reaction is critical since it is part of a chemical cycle that leads to the chemical fixation of CO_2. The three carbon atoms in the dioxolane ring and the attached hydroxyl moiety provide GC with an almost unique number of reactive sites. The hydroxyl group in GC can act as a nucleophile, and the carbon atoms in the ring can act as an electrophile. These reactive sites open up a wide range of possibilities for employing glycerol carbonate as a raw material for converting chemical intermediates into surfactants and polymers. This is an indirect method of synthesizing polymers for application in coatings, adhesives, foams, and other materials [36, 37]. The objective view of this study is the fabrication of a novel membrane buckypaper metal oxide nano-catalysis glycerol carbonate/MWCNTs membrane for the efficient removal of heavy metals from wastewater.

2. Experimental

2.1. Materials and reagents

Pure grade materials were used in the current study including, zinc sulfate heptahydrate ($ZnSO_4.7H_2O$, ≥99%), magnesium acetate tetrahydrate ($(CH3COO)_2Mg.4H_2O$, ≥99%), sodium hydroxide (NaOH, 99%), glycerol (≥99.0%), urea (99%), sulfuric acid (H_2SO_4, 99.9%), hydrochloric acid (HCl, 37%), sodium metaperiodate ($NaIO_4$, 99%), ethylene glycol (98%), sodium thiosulfate ($Na_2S_2O_3$, 99%), potassium iodide (KI, 99.0%), starch, and bromothymol blue. All chemicals were purchased from (Sigma Aldrich, Hamburg, Germany). Grafen Chemical Industries, (Ankara, Turkey), supplied multi-walled carbon nanotubes (MWCNTs, KNT-M31). An immobilon PPVDF membrane with a pore size of 0.45 mm was used as a support layer. It was purchased from Merck KGaA, Germany. Pure metal standards of cadmium, copper, nickel, cobalt, and lead (Cd, Cu, Ni, Co, and Pb) 1000 mg mL^{-1}, nitric acid HNO_3 (2%) were all purchased from PerkinElmer. Milli-Q® water (resistivity of 18.2 MΩ cm) was utilized in the formulation of all solutions in this study.

2.2. Instruments

The Fourier transform infrared spectroscopy (FT-IR, PerkinElmer Ltd, Yokohama, Japan), Ultraviolet and visible spectroscopy (Ultrospec 2100-Biochrom spectrophotometer, (Biochrom Ltd, Cambium, Cambridge, UK), scanning electron microscopy (SEM, JEM-2100F, JEOL Ltd, Tokyo, Japan), X-ray powder diffraction (XRD, PANalyticalX'Pert-PRO, Malvern, United Kingdom), nuclear magnetic resonance (C NMR, H NMR, JNM-ECZR series FT NMR, California, USA), and energy dispersive X-ray (EDX, JSM-7610F; JEOL, Tokyo, Japan) were all applied for the characterization of the synthesized metal oxide nanoparticles.

2.3. Synthesis of ZnO nanoparticles

The synthesis of zinc oxide nanoparticles (ZnONPs) was conducted using the co-precipitation method by the reduction of zinc sulfate heptahydrate with sodium hydroxide. Briefly, 0.1 mol L^{-1} zinc sulfate solution was heated to 100 °C and 0.2 mol L^{-1} NaOH was added dropwise for 30 min. The mixture was heated for 2 h under vigorous magnetic stirring. The resulting solution was lifted aside overnight until the formation of a white precipitate. The formed precipitate was filtered using filter paper Whatman No.1 and washed several times using Milli-Q water. The obtained precipitate was dried at 400 °C in a furnace oven to obtain ZnONPs [38].

2.4. Synthesis of MgO nanoparticles

The co-precipitation method was used for the synthesis of magnesium oxide (MgONPs). At continual stirring, two separate homogeneous aqueous solutions of magnesium acetate (0.2 mol L^{-1}, 50 mL) and Sodium hydroxide (0.4 mol L^{-1}, 50 mL) were prepared. At constant stirring, aqueous sodium hydroxide solution was added drop by drop with aqueous magnesium acetate solution. The color of the fluid changed from transparent to milky white. For 3 h, the mixture was continuously mixed. The solution was then retained for precipitation, and the precipitate was filtered after being washed with Milli-Q water and ethanol numerous times. The entire reaction took place at ambient temperature [39].

2.5. Characterization of metal oxide nanoparticles

The pre-synthesized metal oxide nanoparticles were characterized using different spectroscopic and microscopic techniques. UV-vis spectrophotometer was used to confirm the formation of ZnONPs and MgONPs at the wavelength range of 200–600 nm. FTIR was utilized to determine the possible functional groups that could be present in the formed nanoparticles. XRD analysis was performed to determine the mean average crystallite size. Further investigation was performed under SEM to confirm the size and shape of the pre-synthesized metal oxide nanoparticles. NMR analysis was also performed to know information about the structure and dynamics of components. EDX was used to determine the elemental composition of synthesized nanoparticles and evaluate their purity.

2.6. Synthesis of glycerol carbonate

Glycerol carbonate was synthesized using a three-neck 250 mL flask with a reflux condenser. Briefly, glycerol (10 g) and ZnONPs catalyst (0.3 g) were transferred inside the three-neck flask and heated on a hot plate

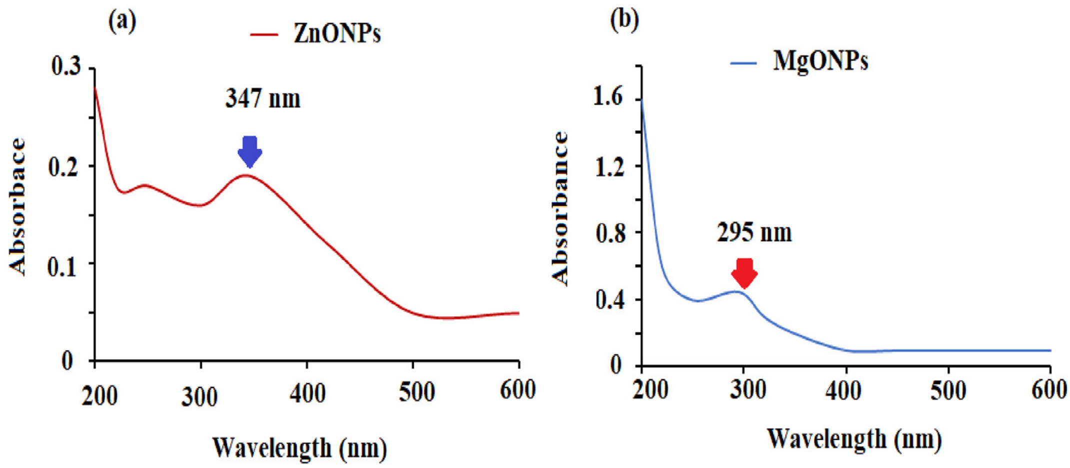

Figure 1. UV-vis spectra of (a) ZnONPs and (b) MgONPs measured at absorption wavelength 200–600 nm.

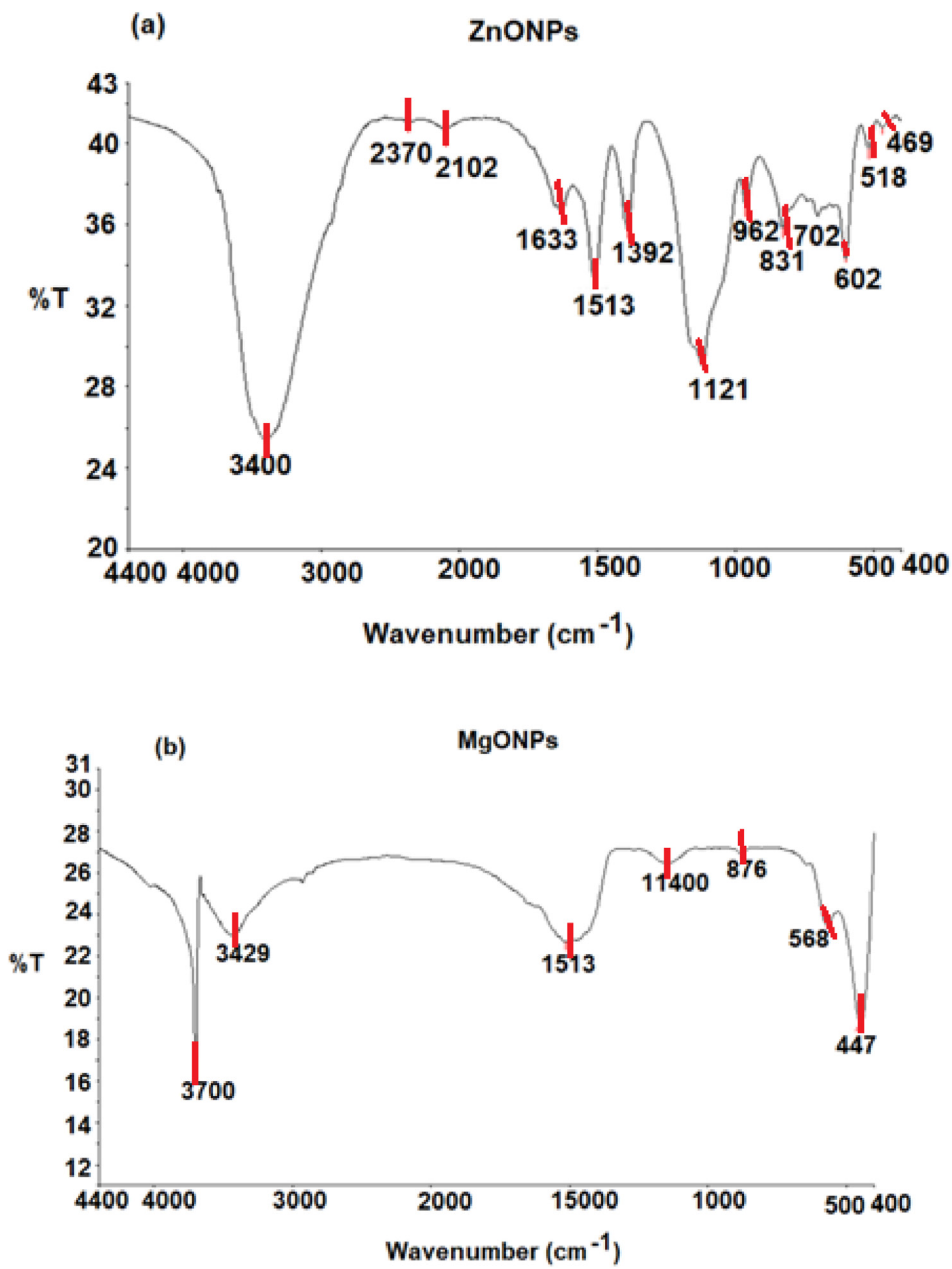

Figure 2. FT-IR spectra of (a) ZnONPs and (b) MgONPs measured at wavenumber in the range of 400–4400 cm^{-1}.

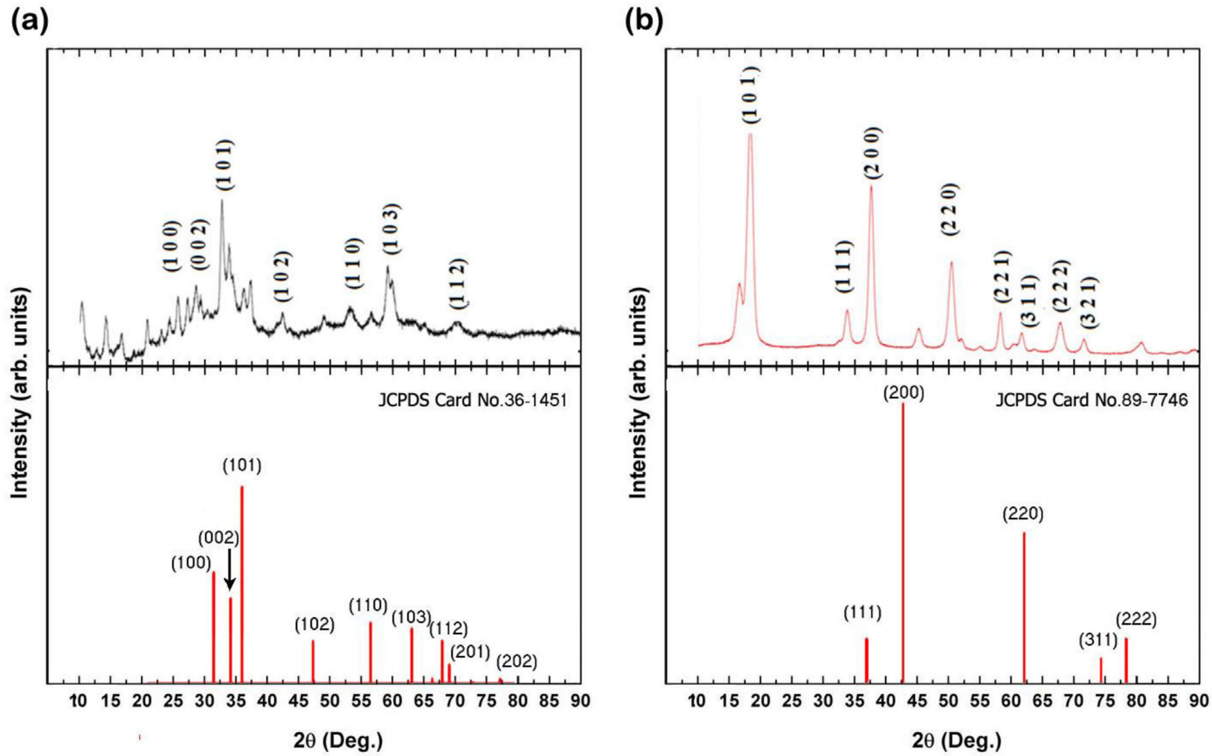

Figure 3. XRD patterns of the synthesized (a) ZnONPs and (b) MgONPs.

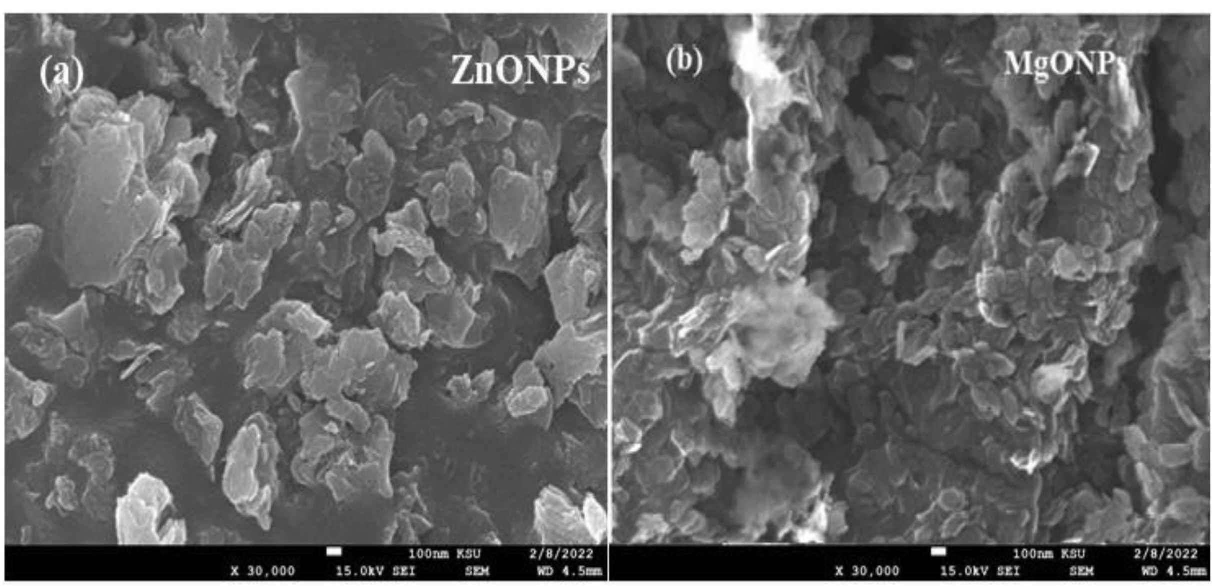

Figure 4. SEM images of (a) ZnONPs and (b) MgONPs synthesized by co-precipitation method.

at 120 °C under constant magnetic stirring, the urea (10 g) was added and the reaction was continued for 4 h. The same procedure was performed for the synthesis of glycerol carbonate in the presence of MgONPs and a catalyst.

2.7. Determination of free glycerol using titration method

The cold oxidation of glycerol by sodium meta periodate in a highly acidic solution is the basis for this test procedure. This process produces formaldehyde and formic acid, which are used to determine the glycerol level by titration with a standard 0.1 mol L^{-1} sodium hydroxide solution.

The titration process was conducted by Pipetting 10 mL of sodium periodate solution (60 g of sodium meta periodate in sufficient water containing 120 mL of 0.1 N sulfuric acid to make 1000 mL) into a 250-measuring flask and diluting with Milli-Q water to the volume and approximately 550 mg of glycerol was added to the flask. Then 50 mL of Milli-Q water was added to the sample followed by the addition of 50 mL of dilute periodate solution. The mixture was kept aside for 30 min. After that, 5 mL of hydrochloric acid and 10 mL of potassium iodide solutions

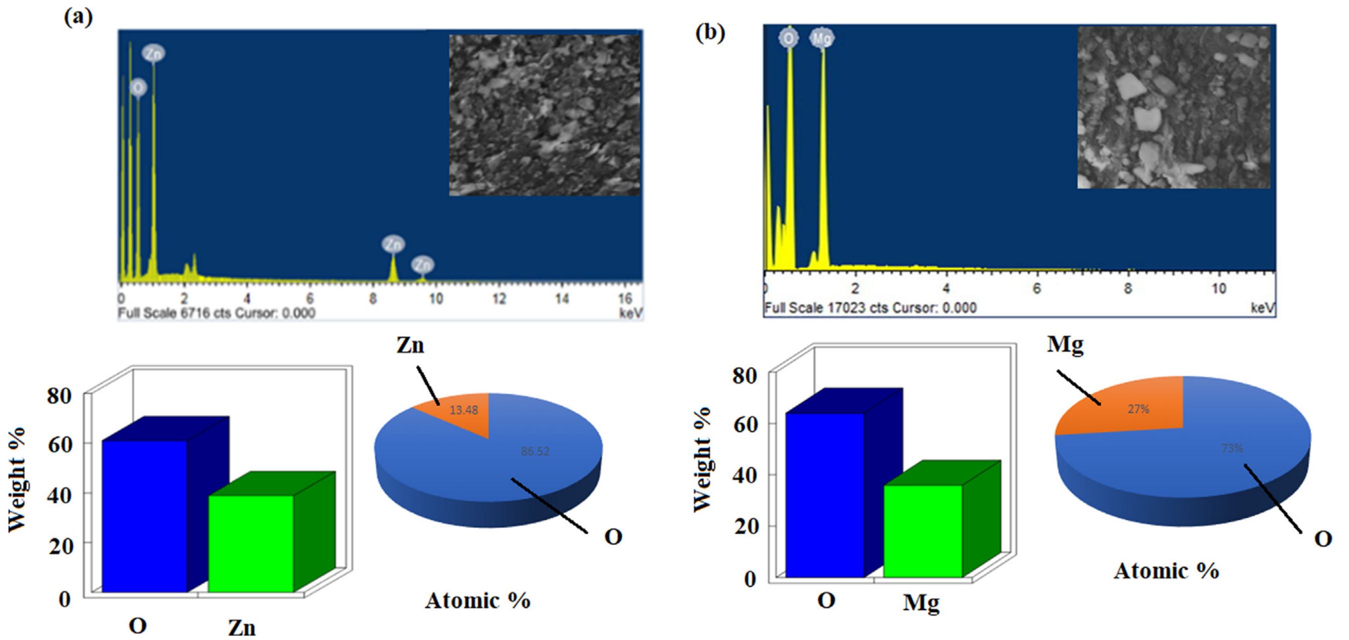

Figure 5. EDX patterns of synthesized metal oxide nanoparticles (a) ZnONPs and (b) MgONPs.

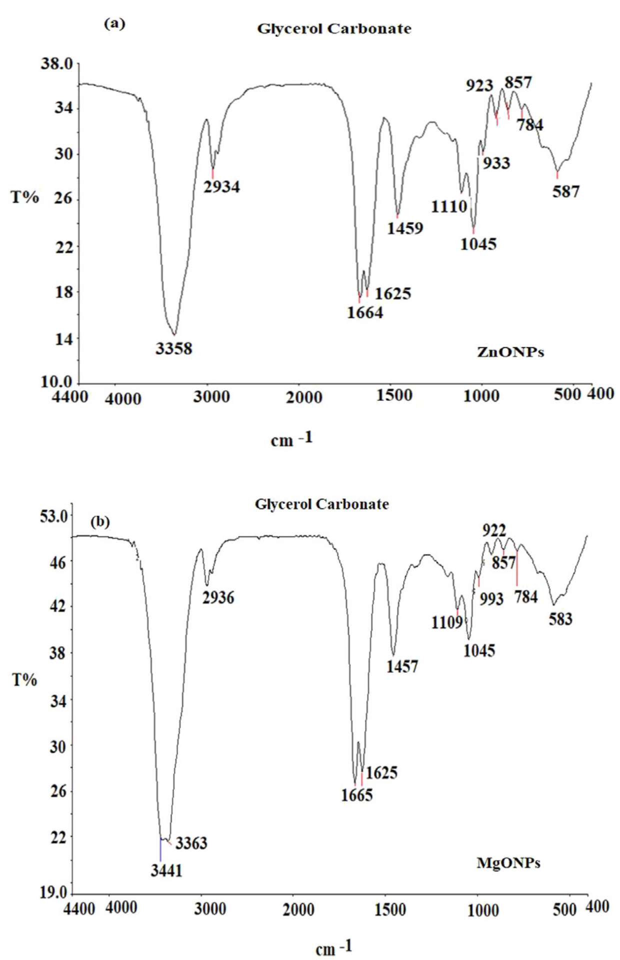

Figure 6. FT-IR of glycerol carbonate in the presence of (a) ZnONPs and (b) MgONPs.

were added. The mixture was gently mixed. The solution was left to stand for 5 min. Then 100 mL of Milli-Q water and 3 mL of starch were added. The titration then was carried out using 0.1 N sodium thiosulfate to the endpoint of starch. The glycerol content is measured in mg/mL. Blank determination was performed by repeating the same procedures using the same amounts of reagents without the test sample. The titration was performed using 0.1 mol L^{-1} sodium hydroxide at pH 6.5.

2.8. Preparation MWTNT/glycerol carbonate dispersed membranes

MWNTs (30 mg) were dispersed using an ultrasonicator (Branson Digital 400W) for 20 min in 30 mL of Milli-Q water with two surfactants (solution1 and solution 2, 2 % w/v). Using a simple filtration vacuum pump, each liquid was diluted to a volume of 0.2 L before being filtered using hydrophilic nylon membrane filters (diameter: 47 mm; pore size: 0.45 m) (CVC2 Vacuubrand). The hydrophilic filtration membrane's surface continued to be covered with MWNTs, creating an extremely thin membrane. The composite membranes were dried for 24 h at 21 °C.

2.9. Characterization of the prepared membranes

The field emission scanning electron microscope examined the morphological characteristics of BP membranes. The JEOL JEC-3000FC fine coater (JOEL. Ltd., Tokyo, Japan) was used to sputter-coat the membranes twice for 30 s after fixing them to various stubs with carbon tape. Following coating, each sample was examined using acceleration voltage in the 5–15 kV range at various magnifications. It is important to note that polymer-based membranes should be rinsed in water for up to 30 min in order to acquire high-quality pictures.

2.10. Heavy metal removal

The Heavy metals rejection of the membranes was evaluated using a dead-end cell. Water was then pumped through the filtration cell using a compressed air cylinder, with membranes that were cut into rectangles (about 4.25 cm^2) and fitted between the two layers of the cell. To control the flow of water through the membranes, varying pressures (1–3 bar) were used. After one hour of filtration testing to establish the steady-state operation, the heavy metal removal sample data were gathered. The feed water for heavy metal removal comprised 6 ppm of a combination of heavy metals at pH 7 (Cd^{+2}, Cu^{+2}, Co^{+2}, Ni^{+2}, and Pb^{+2}). The following Eq. (1) was used to compute the removal of heavy metals:

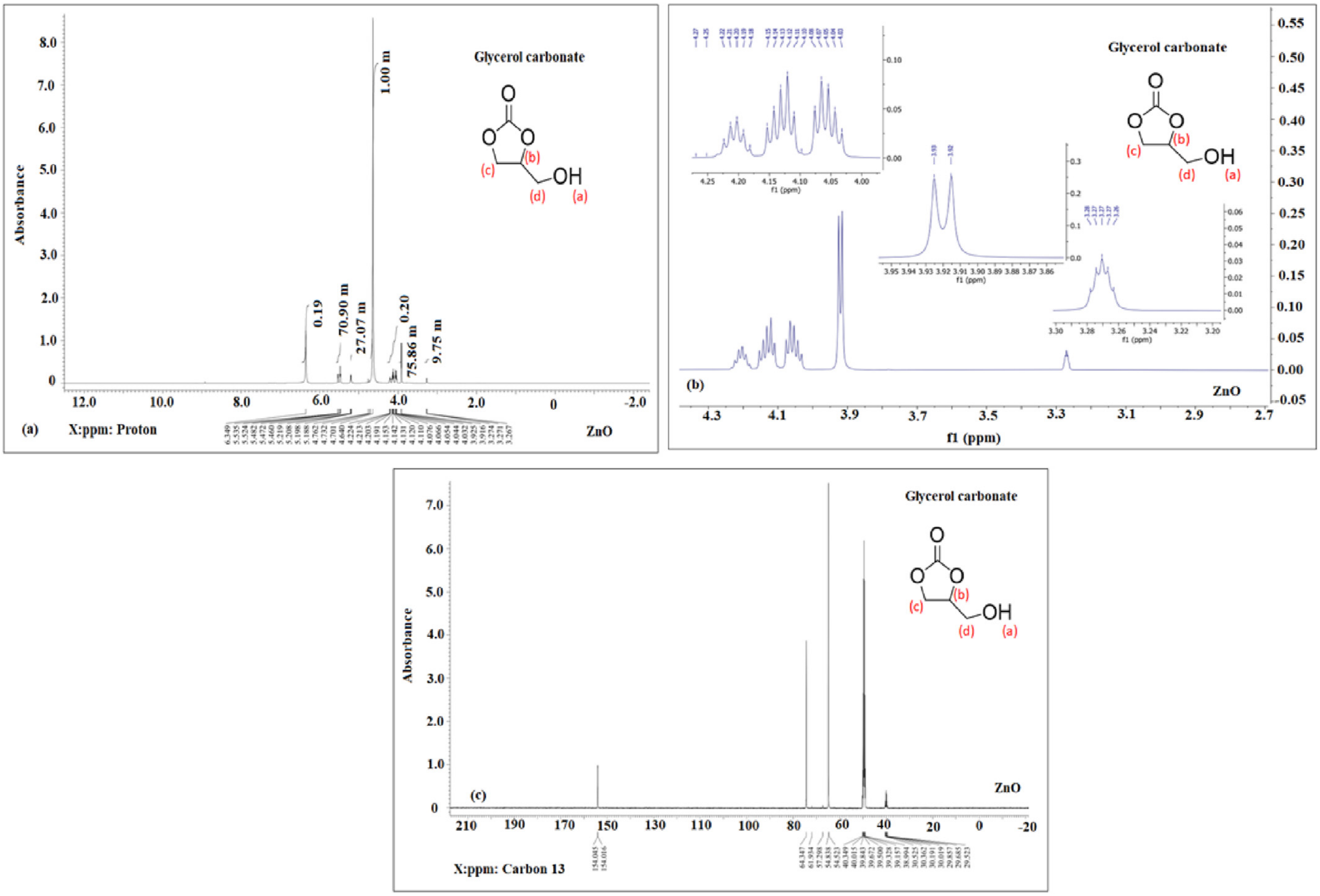

Figure 7. (a & b) ^{1}H-NMR and (c) ^{13}C-NMR for Glycerol carbonate synthesized using ZnO Nano-catalyst.

$$R\% = (1 - Cp/Cf) \times 100\% \tag{1}$$

where Cp and Cf are, respectively, the concentrations of heavy metals in the feed and permeate solutions. By employing ICP-MS Perkin Elmer, inductively coupled plasma atomic emission spectrometry was used to make a quantitative assessment of the removal of heavy metals.

3. Results and discussion

3.1. Characterization of ZnONPs and MgONPs

The size of nanoparticles has a significant impact on the overall characteristics of materials. Thus, studying the size evolution of semiconducting nanoparticles has critical for understanding material characteristics. The technique of UV-visible absorption spectroscopy was commonly utilized to investigate the optical characteristics of nanoscale particles. UV-vis spectroscopy was used to evaluate the optical properties of each produced metal oxide nanoparticle. At 347 nm, a distinct peak attributable to ZnONPs surface plasmon resonance (SPR) was seen (Figure 1a). The absorption spectrum of MgONPs showed the appearance of one peak at 295 nm (Figure 1b). The spectra obtained were found in the agreement with those reported in the literature [40, 41].

FT-IR analysis was utilized to confirm the possible functional groups that can be presented in the formed nanoparticles. The FT-IR spectrum of ZnONPs displayed a chain of absorption bands from 400–4400 cm^{-1}. The absorption band at 3400 was corresponding to the O–H stretching vibration of water. The absorption band at 2370 cm^{-1} corresponds to strong O=C=O carbon dioxide stretching vibration. The observed bands from 1000 to 400 cm^{-1} such as 962, 831, 702, 602, 518, and 469 cm^{-1} correspond to hexagonal crystalline Zn–O nanoparticles (Figure 2a).

MgONPs were analyzed using FT-IR in the 400–4400 cm^{-1} range. Different absorption bands for MgONPs were observed at 3700, 3429, 2362, 1513, 1400, 876, 568, and 447 cm^{-1}. The O–H bond stretching vibration was recorded in two bands at 3700 and 3429 cm^{-1}. CO_2 stretching vibration because of ambient carbon dioxide adsorption was ascribed to the weak band at 2362 cm^{-1}. Two detected absorption bands around 1513 and 1400 cm^{-1}, showed the existence of an O–H stretching mode of water. Magnesium hydroxide (Mg–OH) was found to have a high peak at 876 cm^{-1}. The formation of Mg–O stretching vibrations was corroborated by the observed peaks, which appeared at 568 to 447 cm^{-1} (Figure 2b).

The X-Ray diffraction (XRD) pattern of produced ZnONPs was demonstrated in Figure 3a. The data was collected between the ranges of 20–80 θ and the values were seen in the XRD pattern at 31.84° (1 0 0), 34.52° (0 0 2), 36.38° (1 0 1), 47.64° (1 0 2), 56.7° (1 1 0), 63.06° (1 0 3), and 69.18° (1 1 2) planes. All observed peaks could be hexagonal crystalline and matched the Zinc oxide wurtzite structure (Joint Committee on Powder Diffraction Standards JCPDS Data Card No: 36–1451) [42]. It was also confirmed that the synthesized ZnONPs were free of impurities, as it does not contain any characteristics of XRD peaks other than zinc oxide peaks. The XRD pattern of the synthesized MgO nanoparticles was demonstrated in Figure 3b. The observed peaks appeared at 19.8° (1 0 1), 32.6° (1 1 1), 37.2° (2 0 0), 51.4° (2 2 0), 59.5° (2 2 1), 62.3° (3 1 1), 69.8° (2 2 2), 72.4° (3 2 1). The obtained data showed that the shape of nanoparticles was rod-like structure and these results were in agreement with JCPDS card number 89–7746 [43]. As the width of the peak increases the size of particle size decreases, which resembles that present

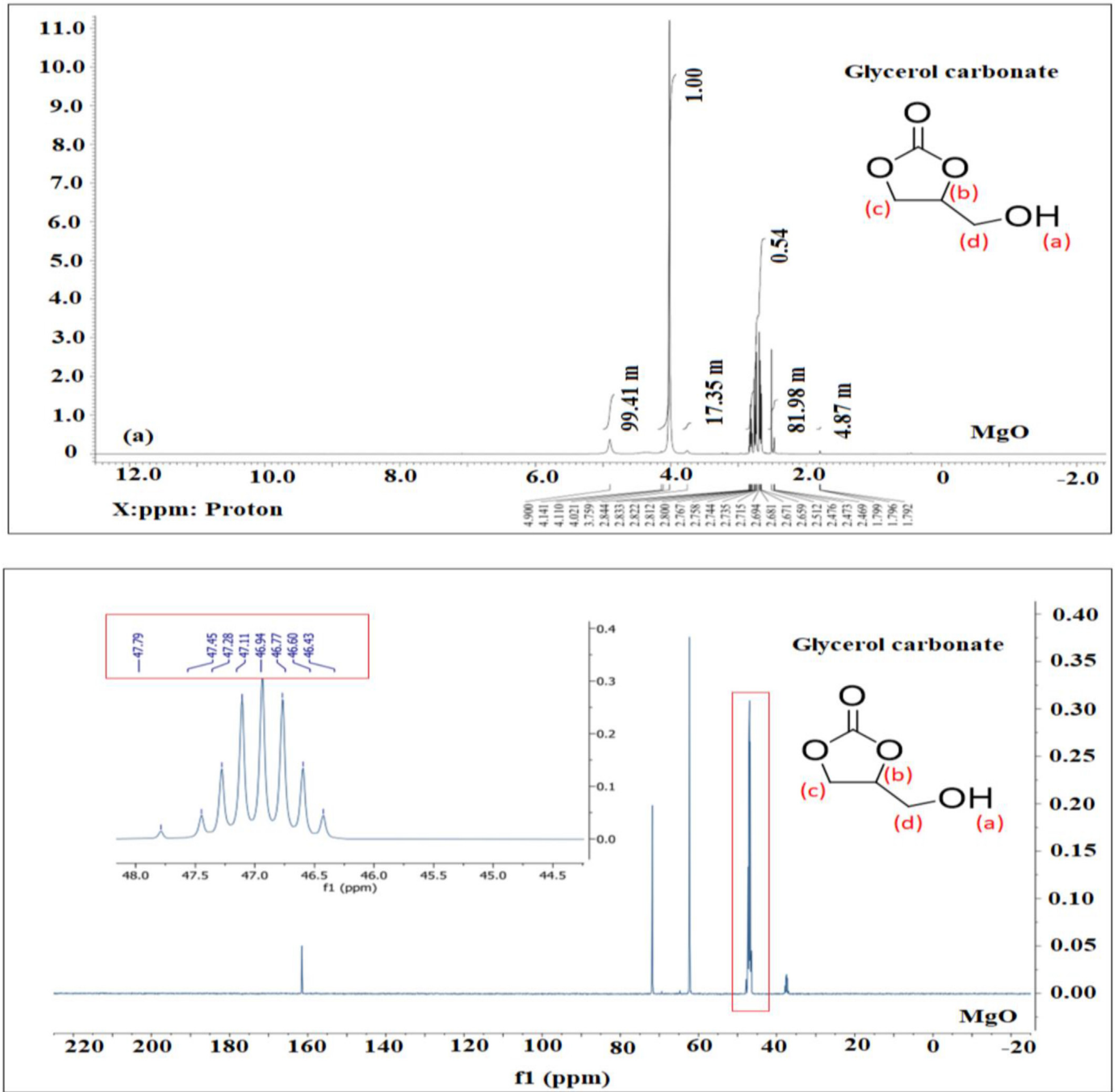

Figure 8. (a) [1]H-NMR and (b) [13]C-NMR for Glycerol carbonate synthesized using MgO Nano-catalyst.

material in the nano range. The prominent peak in the XRD pattern was used to calculate the average crystallite size using a Scherrer formula (2):

$$D = 0.9\lambda / \beta \cos\theta \qquad (2)$$

Where λ, θ and β are the X-ray wavelength, Bragg diffraction angle, and the Full width at half maximum of the XRD peak appearing at a diffraction angle θ, respectively. The average crystallite size of the synthesized ZnONPs and MgONPs was evaluated to be 17.9 ± 1.2 and 25.6 ± 2.5, respectively.

The surface morphology of ZnONPs and MgONPs was examined under SEM using 30,000× magnification. The picked SEM image (Figures 4a and 4b) suggested the formation of stable ZnONPs and MgONPs. The images showed the presence of both individuals as well as the aggregated ZnONPs and MgONPs with particles size ranging from 80–100 nm.

The atomic arrangement of biosynthesized ZnONPs and MgONPs was evaluated by EDX mapping analysis. It was performed to evaluate the chemical contents of the synthesized ZnONPs and MgONPs. The outcomes demonstrated that the weight and atomic percentages of Zn and O in ZnONPs were 61.10% and 38.90% from O and Zn, with atomic percentages of 86.52% and 13.48% from O and Zn, respectively (Figure 5a). However, the elemental composition of the MgONPs showed weight percentages of 64.08%, 35.92% from O and Mg, atomic percentages of 73.05%, and 26.95% from O and Mg (Figure 5b). No additional peaks were recorded relating to other elements, proving the purity of the synthesized ZnONPs and MgONPs.

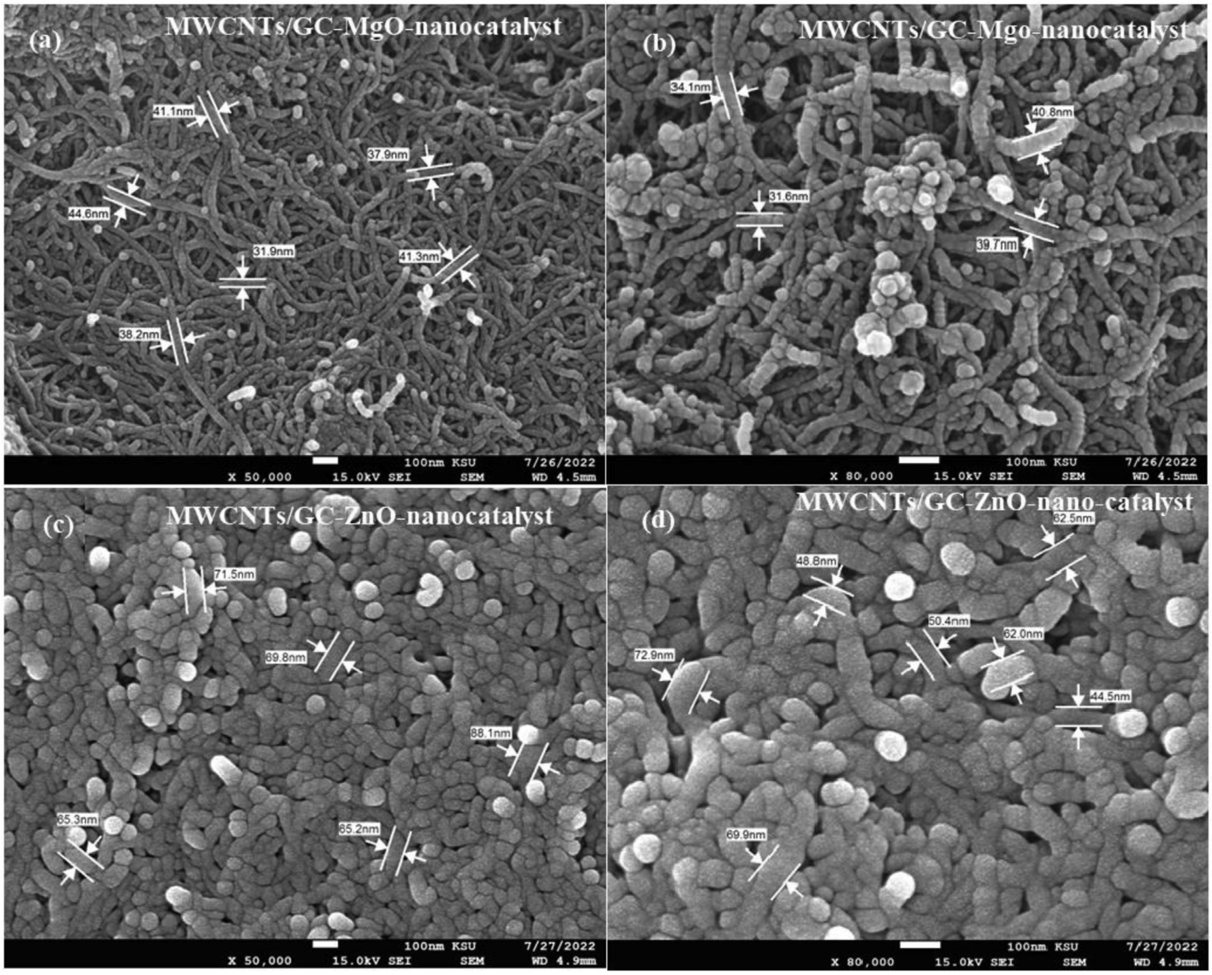

Figure 9. SEM images of (a &b) MWCNTs/GC-MgO-nano-catalyst and (c & d) MWCNTs/GC-ZnO-nano-catalyst buckypaper membranes.

3.2. Synthesis of glycerol carbonate

Trans carbonation is one of the most important routes to produce glycerol carbonate. Glycerol and urea are both inexpensive and affordable reagents and easily available. Urea in this reaction acts as an activated form of CO_2 and an alternative source for carbonylation. Urea is a specifically attractive carbonylating agent due to the only byproduct is ammonia in the gas phase which is easily captured and reused to react with CO_2 forming urea as shown in Eqs. (3) and (4).

$$2NH_3 + CO_2 \rightleftharpoons NH_2COONH_4 \tag{3}$$

$$NH_2COONH_4 \rightleftharpoons CO(NH_2)_2 + H_2O \tag{4}$$

The formation of glycerol carbonate takes place without any solvents. Although the synthesis of glycerol carbonate from urea and glycerol can be accelerated by increasing the temperature, several catalysts have been discovered to improve the reaction's rate and selectivity. Metallic oxide nanoparticles such as ZnONPs and MgONPs were used as catalytic agents in the formation of glycerol carbonate.

3.3. Confirmation of glycerol carbonate using FT-IR analysis

FT-IR analysis was utilized to characterize the functional groups of glycerol carbonate that were pre-synthesized using ZnONPs or MgONPs. The FT-IR spectrum of glycerol carbonate displayed various vibration bands at 3358 (OH stretching vibration), 2934 (N–H strong stretching vibration), 1664 (C–H bending), 1625 (medium N–H bending amine), 1459 (C–H bending vibration), 1110, 1045 (strong CO–O–CO), 933–587 (Zn–O) cm^{-1} (Figure 6a). However, the FT-IR spectrum (Figure 6b) showed nearly the same vibration bends with slight changes. Two absorption bands were observed at 3441 and 3363 cm^{-1} corresponding to the (O–H stretching vibration of water and N–H stretching vibration of amine), respectively. Different vibration bands appeared at 1665, 1625,1457, 1109, and 1045 cm^{-1} corresponding to C–H bending, N–H bending amine, C–H, bending, and CO–O–CO vibrations, respectively. The bands in the range from 1000–400 correspond to the presence of metal oxide (Mg–O).

3.4. Confirmation of glycerol carbonate formations using NMR

3.4.1. Nuclear magnetic resonance (^{13}C NMR) and (^{1}H NMR) for glycerol carbonate synthesized using ZnO nano-catalyst

The formed GC using nano-catalyst ZnO was confirmed through ^{1}HNMR and ^{13}C NMR. The ^{1}H-NMR spectrum of the synthesized GC using ZnONPs showed the absence of glycerol protons as no signals were detected in the range 3.3–3.5 ppm (Figures 7a and 7b). The glycerol carbonate ^{1}H-NMR spectrum detected a signal at $\delta H = 3.9$ ppm for traces of residual ethanol protons. The spectrum recorded a plot of characteristic signals of GC characteristic protons. A multiple signal at 4.05 and 4.1 ppm refers to proton (d). The quartet peak at $\delta H = 5.2$ ppm represents proton (c). The triplet and doublet appear at $\delta H = 5.5$ ppm representing CH proton (b). Finally, the signal observed at $\delta H = 6.4$ ppm was assigned to OH proton (a).

The ^{13}C spectrum of the synthesized GC using nano-catalyst ZnO displayed significant characteristics of glycerol carbonate signals that derived from cyclic carbon atoms as well as linear carbonate signals

160.9 ppm, 72.9 ppm, 66.7 ppm, and 63.45 ppm. These results are in agreement with the previously reported results [44]. The linear carbonate atoms were located at 66.7 ppm and 72.90 ppm. These results suggested the efficient catalytic pathway for the formation of cyclic carbonates such as GC and linear carbonate (Figure 7c).

3.4.2. Nuclear magnetic resonance (^{1}H NMR) and (^{13}C NMR) for glycerol carbonate synthesized using MgO nano-catalyst

The ^{1}H-NMR spectrum of glycerol carbonate synthesized using MgONPs confirmed the identity of the GC by showing all its distinguishing signals in Figure 8a. ^{1}H NMR (400 MHz, DMSO-d_6) exhibited three multiple signals at δH = 2.65, 2.75, and 2.8 ppm which are corresponding to protons (d), (c), and (b) respectively. The characteristic signal at δH = 4.9 ppm points to OH proton (a).

The ^{13}C spectrum of the synthesized GC using nano-catalyst MgO displayed significant characteristics of glycerol carbonate signals that derived from cyclic carbon atoms as well as linear carbonate signals 154 ppm, 64.3 ppm, 54.5 ppm, and 43.9 ppm. These results are in agreement with the previously reported results [44]. The linear carbonate atoms were located at 64.3 ppm and 72.90 ppm. These results suggested the efficient catalytic pathway for the formation of cyclic carbonates such as GC and linear carbonate (Figure 8b).

3.5. Determination of total yield of free glycerol

The content of glycerol estimated as a percentage, is calculated by the following Eq. (5):

$$\text{Glycerol } (\%) = (V_1\text{-}V_B) \times F \times N/W \tag{5}$$

Where VB is the volume of 0.1 N sodium hydroxide solution used for the blank titration and V1 is the volume of 0.1 N sodium hydroxide solution used for the sample titration, F = 9.210, N = precise normality of the sodium hydroxide used for titration, and M = mass of glycerin subjected to reaction with sodium meta periodate solution (in grammes). The results revealed that the sample's titration volume for the ZnO nano-catalyst-generated sample was 2.6 mL as shown in Eq. (6).

$$\text{Glycerol } (\%) = \frac{(2.6 - 7.5) \times 9.210 \times 0.1}{0.55} = 8.21\% \tag{6}$$

Meanwhile, the volume of titration for the sample synthesized using MgO nano-catalyst = 5.4 mL as shown in Eq. (7).

$$\text{Glycerol } (\%) = \frac{(5.4 - 7.5) \times 9.210 \times 0.1}{0.55} = 3.52\% \tag{7}$$

3.6. Morphological characteristics of the fabricated membranes

A reliable indicator of the structure and porosity of membranes is their shape. It indicates the membrane's flow, size distribution, and pore geometry. The materials and fabrication methods utilized have an impact on the shape of membranes, among other things. The surface SEM images of the MWCNTs/GC BP membranes were obtained. uniformly distributed MWCNTs over the BP membrane's flat, homogeneous surface (Figures 9a and 9b) for SEM images of MWCNTs/GC-MgO-nano-catalyst and (Figures 9c and 9d) for MWCNTs/GC-ZnO-nano-catalyst buckypaper membranes.

3.7. Contact angle

The hydrophilicity-hydrophobicity of a solid surface can be determined by using the static contact-angle technique [45]. A surface's hydrophobicity will also decrease if the contact angle lowers for that surface, and vice versa. Since the hydrophilicity/hydrophobicity of a membrane affects how the membrane interacts with water, organic compounds, and inorganic materials, contact angle was regarded as a standard measurement for membranes [46]. MWCNTs display a hydrophobic property by nature [47]. However, as stated by previous researchers who utilized surfactants and other polymers, it is anticipated that their dispersion with polymers will diminish the hydrophobicity [13]. It is crucial to understand that glycerol carbonate, which is used in this study acts as a surfactant, is used to permeabilize organic membranes, and is utilized as a dispersion in the two membranes. The contact angle of MWCNTs/GC-MgO-nano-catalyst and MWCNTs/GC-ZnO -nano-catalyst BP membranes were found as 63.72 ± 1.78 and 65.46 ± 2.69, respectively.

Adsorption, which can happen for a number of reasons, including van der Waals interactions, hydrogen bonds, and electrostatic attraction, may also have an impact on how metal ions are rejected [48]. The results showed that both membranes displayed excellent metal rejection rates up to 99% for the tested ions (Cd^{2+}, Cu^{2+}, Co^{2+}, Ni^{2+}, and Pb^{2+}) at pH 7 and ambient temperature. The effect of applied pressure on the heavy metal ions rejection rate of both MWCNTs/GC-MgO-nano-catalyst and MWCNTs/GC-ZnO-nano-catalyst BP is demonstrated in Figures 10a and 10b. The results showed that the MWCNTs/GC-ZnO-nano-catalyst exhibited high efficiency for the removal of $Pb^{2+} > Cu^{2+} > Cd^{2+} > Co^{2+} > Ni^{2+}$, and the MWCNTs/GC-MgO-nano-catalyst exhibited high efficiency for the removal of $Ni^{2+} > Co^{2+} > Cd^{2+} > Cu^{2+} > Pb^{2+}$.

3.8. Heavy metal removal

The size exclusion mechanism is more likely to play a role in the rejection of heavy metals by BP membranes than any other membrane filtration process. For both membranes, cylindrical carbon tubes were stable with pressure. However, as the pressure increased, the rejection rate of the remaining metal ions either decreased or stayed steady without significantly changing.

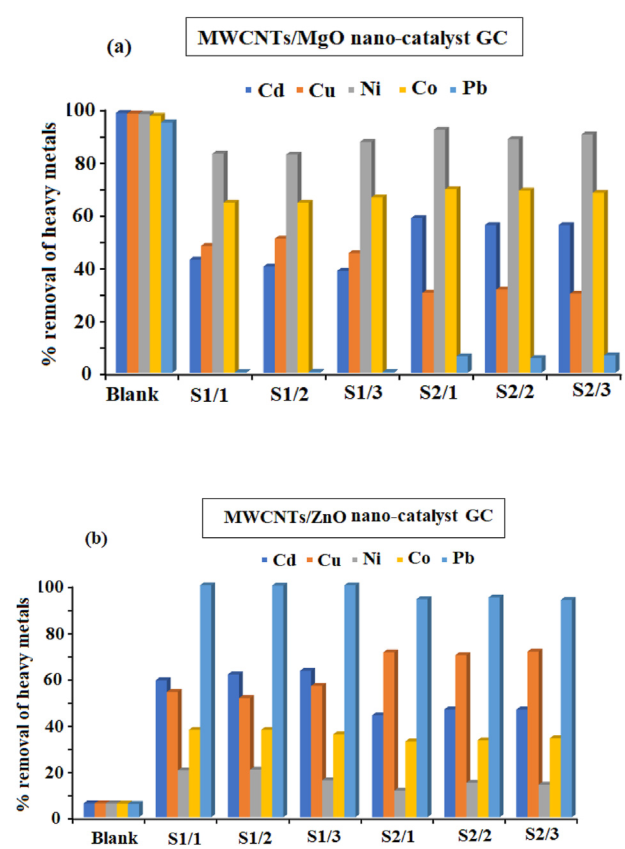

Figure 10. The percentage removal of heavy metals using (a) MWCNTs/MgO nano-catalyst GC and (b) MWCNTs/ZnO nano-catalyst GC buckypaper membranes.

The rejection of metal ions was more efficient in MWCNTs/GC-ZnO-nano-catalyst compared to the MWCNTs/GC-MgO-nano-catalyst membrane.

4. Conclusion

The production of two metal oxide nanoparticles (ZnONPs and MgONPs) has been accomplished using a straightforward co-precipitation technique. The creation of nanoparticles was verified using a variety of spectroscopic and microscopic techniques. The results showed that hexagonal and cubic nanostructured metal oxides with high purity and particle sizes of about 100 nm were prepared. The reaction between glycerol and urea to form glycerol carbonate has been used to test the catalytic effectiveness of the pre-synthesized metal oxide nanoparticles. The results showed that adding ZnONPs and MgONPs catalytic agents significantly increased the synthesis of glycerol carbonate while exhibiting outstanding activity as nano-catalysts. The generated glycerol carbonate was used to create two BP membranes for the rejection of heavy metals (Cd^{2+}, Cu^{2+}, Co^{2+}, Ni^{2+}, and Pb^{2+}) using MWCNTs/GC-ZnO and MWCNTs/GC-MgO nano-catalyst, respectively. The as-constructed BP membranes were characterized by SEM. The documented enhancement in membrane performance and properties proved the necessity of using these fillers. Fillers changed the morphology of membranes, increasing their porosity and the effectiveness of rejection. Both membranes also have effective qualities that are suitable for filtration processes at low pressures. The results of this study also show that BP membrane systems are a desired issue for other researchers to study in order to deepen our understanding of preferred membranes, especially the selective uptake of heavy metal ions.

Declarations

Author contribution statement

Seham S. Alterary: Conceived and designed the experiments; Performed the experiments; Analyzed and interpreted the data; Contributed reagents, materials, analysis tools or data; Wrote the paper.

Ahmed A. Alshahrani: Analyzed and interpreted the data; Contributed reagents, materials, analysis tools or data; Wrote the paper.

Shahad A. Alsahli: Performed the experiments; Analyzed and interpreted the data; Contributed reagents, materials, analysis tools or data; Wrote the paper.

Funding statement

This work was supported by Researchers Supporting Project in King Saud University (RSP-2021/195).

Data availability statement

Data included in article/supplementary material/referenced in article.

Declaration of interest's statement

The authors declare no conflict of interest.

Additional information

No additional information is available for this paper.

References

[1] M. Mary Theresa, Eric MV. Hoek, A review of water treatment membrane nanotechnologies, Energy Environ. Sci. 4 (6) (2011) 1946e71.

[2] P.H. Raven, D.L. Wagner, Agricultural intensification and climate change are rapidly decreasing insect biodiversity, Proc. Natl. Acad. Sci. USA 118 (2) (2021), e2002548117.

[3] M. Sajid, M.K. Nazal, N. Baig, A.M. Osman, Removal of heavy metals and organic pollutants from water using dendritic polymers-based adsorbents: a critical review, Separ. Purif. Technol. 191 (2018) 400e23.

[4] H.M. Tauqeer, V. Turan, M. Iqbal, Production of safer vegetables from heavy metals contaminated soils: the current situation, concerns associated with human health and novel management strategies, in: Advances in Bioremediation and Phytoremediation for Sustainable Soil Management, 2022, pp. 301–312.

[5] P. Gao, J. Cui, Y. Deng, Direct regeneration of ion exchange resins with sulfate radical-based advanced oxidation for enabling a cyclic adsorption–regeneration treatment approach to aqueous perfluorooctanoic acid (PFOA), Chem. Eng. J. 405 (2021 Feb 1), 126698.

[6] L. Huang, H. Wan, S. Song, D. Liu, G.L. Puma, Complete removal of heavy metals with simultaneous efficient treatment of etching terminal wastewater using scaled-up microbial electrolysis cells, Chem. Eng. J. 439 (2022), 135763.

[7] Z. Xu, Q. Zhang, X. Li, X. Huang, A critical review on chemical analysis of heavy metal complexes in water/wastewater and the mechanism of treatment methods, Chem. Eng. J. 429 (2022), 131688.

[8] F. Zhu, Y.M. Zheng, B.G. Zhang, Y.R. Dai, A critical review on the electrospun nanofibrous membranes for the adsorption of heavy metals in water treatment, J. Hazard Mater. 401 (2021), 123608.

[9] S. Han, W. Li, H. Xi, R. Yuan, J. Long, C. Xu, Plasma-assisted in-situ preparation of graphene-Ag nanofiltration membranes for efficient removal of heavy metal ions, J. Hazard Mater. 423 (2022), 127012.

[10] B.Q. Huang, Y.J. Tang, A.R. Gao, Z.X. Zeng, S.M. Xue, C.H. Ji, C.Y. Tang, Z.L. Xu, Dually charged polyamide nanofiltration membranes fabricated by microwave-assisted grafting for heavy metals removal, J. Membr. Sci. 640 (2021), 119834.

[11] A.A. Alshahrani, M. AlQahtani, A.M. Almushaikeh, H.M. Hassan, M. Alzaid, A.N. Alrashidi, I.H. Alsohaimi, Synthesis, characterization, and heavy-ion rejection rate efficiency of PVA/MWCNTs and Triton X-100/MWCNTs Buckypaper membranes, J. Mater. Res. Technol. 18 (2022) 2310–2319.

[12] B. Ye, C. Jia, Z. Li, L. Li, Q. Zhao, J. Wang, H. Wu, Solution-blow spun PLA/SiO2 nanofiber membranes toward high efficiency oil/water separation, J. Appl. Polym. Sci. 137 (37) (2020), 49103.

[13] A.A. Alshahrani, M. AlQahtani, A.M. Almushaikeh, H.M. Hassan, M. Alzaid, A.N. Alrashidi, et al., Synthesis and characterization of MWCNTS/chitosan and MWCNTS/chitosan-crosslinked Buckypaper membranes for desalination, Desalination 418 (2017) 60e70.

[14] S. Kang, M. Herzberg, D.F. Rodrigues, M. Elimelech, Antibacterial effects of carbon nanotubes: size does matter, Langmuir 24 (13) (2008) 6409e13.

[15] S.M. Imran, G.N. Shao, M.S. Haider, H.J. Hwang, Y.H. Choa, M. Hussain, H.T. Kim, Carbon nanotube-based thermoplastic polyurethane-poly (methyl methacrylate) nanocomposites for pressure sensing applications, Polym. Eng. Sci. 56 (9) (2016) 1031–1036.

[16] A.A. Alshahrani, M. AlQahtani, A.M. Almushaikeh, H.M. Hassan, M. Alzaid, A.N. Alrashidi, et al., The rejection of mono-and divalent ions from aquatic environment by MWCNTS/chitosan buckypaper composite membranes: influences of chitosan concentrations, Separ. Purif. Technol. 234 (2020), 116088.

[17] R. Das, M.E. Ali, S.B. Abd Hamid, S. Ramakrishna, Z.Z. Chowdhury, Carbon nanotube membranes for water purification: a bright future in water desalination, Desalination 336 (2014) 97e109.

[18] G. Baskar, A. Gurugulladevi, T. Nishanthini, R. Aiswarya, K.J. Tamilarasan, Optimization and kinetics of biodiesel production from Mahua oil using manganese doped zinc oxide nanocatalyst, Renew. Energy 103 (2017) 641–646.

[19] R. Koutavarapu, M.R. Tamtam, M.C. Rao, S.G. Peera, J. Shim, Recent progress in transition metal oxide/sulfide quantum dots-based nanocomposites for the removal of toxic organic pollutants, Chemosphere 272 (2021), 129849.

[20] P. Cheng, X. Zhao, H. El-Ramady, T. Elsakhawy, M.G. Waigi, W. Ling, Formation of environmentally persistent free radicals from photodegradation of triclosan by metal oxides/silica suspensions and particles, Chemosphere 290 (2022), 133322.

[21] M.M. Ghafurian, F. Dastjerd, A. Afsharian, F.R. Esfahani, H. Niazmand, H. Behzadnia, S. Wongwises, O. Mahian, Low-cost zinc-oxide nanoparticles for solar-powered steam production: superficial and volumetric approaches, J. Clean. Prod. 280 (2021), 124261.

[22] S. Choudhary, A. Sachdeva, P. Kumar, Time-based assessment of thermal performance of flat plate solar collector using magnesium oxide nanofluid, Int. J. Sustain. Energy 40 (5) (2021 May 28) 460–476.

[23] C. Karthikeyan, N. Sisubalan, M. Sridevi, K. Varaprasad, M.H. Basha, W. Shucai, R. Sadiku, Biocidal chitosan-magnesium oxide nanoparticles via a green precipitation process, J. Hazard Mater. 411 (2021 Jun 5), 124884.

[24] B. Sachuthananthan, R.L. Krupakaran, G. Balaji, Exploration on the behaviour pattern of a DI diesel engine using magnesium oxide nano additive with plastic pyrolysis oil as alternate fuel, Int. J. Ambient Energy 42 (6) (2021) 701–712.

[25] M.S. Kumar, R. Rajasekar, S. Ganesan, S.P. Venkatesan, V.P. Kumar, Evaluation of metal oxide nano particles in lemongrass biodiesel for engine performance, emission and combustion characteristics, Mater. Today Proc. 44 (2021) 3657–3665.

[26] Z. Xu, Z. Li, Dynamic humidity response of surface acoustic wave sensors based on zinc oxide nanoparticles sensitive film, Appl. Phys. A 127 (6) (2021) 1–7.

[27] A.G. El-Shamy, New nano-composite based on carbon dots (CDots) decorated magnesium oxide (MgO) nano-particles (CDots@ MgO) sensor for high H2S gas sensitivity performance, Sensor. Actuator. B Chem. 329 (2021), 129154.

[28] F. Faizah, B. Priyono, Z.E. Chairunnisa, M.R. Nugraha, A.Z. Syahrial, A. Subhan, Zinc Oxide Nanoparticle and its characterization in the LTO/ZnO composite for

lithium-ion battery anode, InIOP Conf. Ser.: Mater. Sci. Eng. 1098 (6) (2021), 062027. IOP Publishing.
[29] M. Mansour, M. Eleraki, A. Noah, E.A. Moustafa, Using nanotechnology to prevent fines migration while production, Petroleum 7 (2) (2021) 168–177.
[30] S. Jadoun, J. Yáñez, H.D. Mansilla, U. Riaz, N.P. Chauhan, Conducting polymers/zinc oxide-based photocatalysts for environmental remediation: a review, Environ. Chem. Lett. (2022 Feb 19) 1–21.
[31] K. Tharani, A.J. Christy, S. Sagadevan, L.C. Nehru, Fabrication of Magnesium oxide nanoparticles using combustion method for a biological and environmental cause, Chem. Phys. Lett. 763 (2021), 138216.
[32] D. Murguía-Ortiz, I. Cordova, M.E. Manriquez, E. Ortiz-Islas, R. Cabrera-Sierra, J.L. Contreras, B. Alcántar-Vázquez, M. Trejo-Rubio, J.T. Vázquez-Rodríguez, L.V. Castro, Na-CaO/MgO dolomites used as heterogeneous catalysts in canola oil transesterification for biodiesel production, Mater. Lett. 291 (2021), 129587.
[33] S. Nomanbhay, M.Y. Ong, K.W. Chew, P.L. Show, M.K. Lam, W.H. Chen, Organic carbonate production utilizing crude glycerol derived as by-product of biodiesel production: a review, Energies 13 (6) (2020) 1483.
[34] N.A. Zuhaimi, V.P. Indran, M.A. Deraman, N.F. Mudrikah, G.P. Maniam, Y.H. Taufiq-Yap, M.H. Rahim, Reusable gypsum based catalyst for synthesis of glycerol carbonate from glycerol and urea, Appl. Catal. Gen. 502 (2015) 312–319.
[35] M.O. Sonnati, S. Amigoni, E.P. de Givenchy, T. Darmanin, O. Choulet, F. Guittard, Glycerol carbonate as a versatile building block for tomorrow: synthesis, reactivity, properties and applications, Green Chem. 15 (2) (2013) 283–306.
[36] R. Morales-Cerrada, B. Boutevin, S. Caillol, Glycerol carbonate methacrylate: a cross-linking agent for hydroxyurethane-acrylate coatings, Prog. Org. Coating 151 (2021 Feb 1), 106078.
[37] M. Malyaadri, K. Jagadeeswaraiah, P.S. Prasad, N. Lingaiah, Synthesis of glycerol carbonate by transesterification of glycerol with dimethyl carbonate over Mg/Al/Zr catalysts, Appl. Catal. Gen. 401 (1-2) (2011) 153–157.
[38] E.F. El-Belely, M.M. Farag, H.A. Said, A.S. Amin, E. Azab, A.A. Gobouri, A. Fouda, Green synthesis of zinc oxide nanoparticles (ZnONPs) using Arthrospira platensis (Class: Cyanophyceae) and evaluation of their biomedical activities, Nanomaterials 11 (1) (2021 Jan 4) 95.
[39] M.M. Rahman, J. Ahmed, A.M. Asiri, S.Y. Alfaifi, Ultra-sensitive, selective and rapid carcinogenic Bisphenol A contaminant determination using low-dimensional facile binary Mg-SnO_2 doped microcube by potential electro-analytical technique for the safety of environment, J. Ind. Eng. Chem. 109 (2022) 147–154.
[40] B.N. Patil, T.C. Taranath, Limonia acidissima L. leaf mediated synthesis of zinc oxide nanoparticles: a potent tool against Mycobacterium tuberculosis, Int. J. Mycobacter. 5 (2) (2016) 197–204.
[41] T. Somanathan, V.M. Krishna, V. Saravanan, R. Kumar, R. Kumar, MgO nanoparticles for effective uptake and release of doxorubicin drug: pH sensitive controlled drug release, J. Nanosci. Nanotechnol. 16 (9) (2016) 9421–9431.
[42] N.P. Subiramaniyam, S. Vadivel, S. Kumaresan, K. Vallalperuman, Fluorine-doped nanocrystalline ZnO powders prepared via microwave irradiation route as effective materials for photocatalyst, J. Mater. Sci. Mater. Electron. 28 (21) (2017) 16173–16180.
[43] M. Kalaimathi, K. Hariharan, S. Vishnu, R. Chinnasamy, Parallel synthesis and optimization of magnesium oxide nanoparticles using Tridax procumbens and Myristica fragrance, Curr. Res. Green Sustain. Chem. 4 (2021), 100185.
[44] M. Aresta, A. Dibenedetto, L. Di Bitonto, New e)cient and recyclable catalyst for the synthesis of di- and tri-glycerol carbonates, RSC Adv. 5 (2015) 64433–66443.
[45] S. Kar, R.C. Bindal, P.K. Tewari, Carbon nanotube membranes for desalination and water purification: challenges and opportunities, Nano Today 7 (2012) 385e9.
[46] B. Ribeiro, E.C. Botelho, M.L. Costa, C.F. Bandeira, Carbon nanotube buckypaper reinforced polymer composites: a review, Polıámeros 27 (2017) 247e55.
[47] K. Sears, L. Dumee, J. Schu ̈tz, M. She, C. Huynh, S. Hawkins, et al., Recent developments in carbon nanotube membranes for water purification and gas separation, Materials 3 (1) (2010) 127e49.
[48] Md Rashid, S.F. Ralph, Carbon nanotube membranes: synthesis, properties, and future filtration applications, Nanomaterials 7 (5) (2017) 99.